Kinetic and Mechanistic Studies of Vanadium-Based, Extended Catalytic Lifetime Catechol Dioxygenases

Cindy-Xing Yin and Richard G. Finke*

Contribution from the Department of Chemistry, Colorado State University, Fort Collins, Colorado 80523

Received May 7, 2005; E-mail: rfinke@lamar.colostate.edu

Abstract: Recently we showed that V-containing polyoxometalates such as $(n\text{-Bu}_4\text{N})_7\text{SiW}_9\text{V}_3\text{O}_{40}$ or $(n\text{-Bu}_4\text{N})_9\text{P}_2\text{W}_{15}\text{V}_3\text{O}_{62}$, as well as eight other V-containing precatalysts tested, evolve to high-activity, long catalytic lifetime ($\geq$ 30 000$-$100 000 total turnovers) 3,5-di-*tert*-butylcatechol (DTBC) dioxygenases in which Pierpont's complex [VO(DBSQ)(DTBC)]$_2$ is apparently a common catalyst resting state [Yin, C.-X.; Finke, R. G. *J. Am. Chem. Soc.* **2005**, *107*, 9003$-$9013]. In a separate paper, autoxidation of DTBC to the corresponding benzoquinone and H_2O_2 was shown to be a key to the catalyst evolution process: the H_2O_2, DTBC, and O_2 plus virtually any V-based precatalyst tested form [VO(DBSQ)(DTBC)]$_2$ under the catalytic conditions, that catalyst formation process being autocatalytic in H_2O_2. The resulting novel concept is that of an autoxidation-product-initiated dioxygenase [Yin, C.-X.; Sasaki, Y.; Finke, R. G. *Inorg Chem.* **2005**, in press]. Herein the following questions about this record catalytic lifetime 3,5-di-*tert*-butylcatechol dioxygenase catalyst are explored: (i) What is the rate law for 3,5-di-*tert*-butylcatechol dioxygenation when one *begins* with Pierpont's [VO(DBSQ)(DTBC)]$_2$? (ii) Does it support the hypothesis that this complex is a catalyst resting state or, perhaps, even the true catalyst? (iii) Can a mechanism be written from that information and from the knowledge in the dioxygenase literature? The results answer each of these questions and provide considerable mechanistic insight into the most catalytically active and long-lived DTBC dioxygenase catalyst presently known.

Introduction

Recently we extended our 1999 findings[1] by reporting[2] that virtually any vanadium-based precursor tested evolved into a highly effective dioxygenase-type oxidative cleavage catalyst for 3,5-di-*tert*-butylcatechol (hereafter DTBC) dioxygenation with O_2 to yield the products shown in Scheme 1.[1-3] A record $\geq$ 100 000 total turnover (TTO) catalytic lifetimes[1] were observed en route to oxidative ring-cleavage products, **2**–**5**, plus the autoxidation product, **6** (Scheme 1).[1-3]

Electron paramagnetic resonance (EPR) spectroscopy, negative ion electrospray ionization mass spectrometry (ESI-MS), catalytic activity, selectivity, and lifetime studies revealed that Pierpont's crystallographically characterized vanadium semiquinone catecholate dimer complex, [VO(DBSQ)(DTBC)]$_2$ (where DBSQ is 3,5-di-*tert*-butylsemiquinone and DTBC is the 3,5-di-*tert*-butylcatecholate dianion), is either the catalyst resting state or possibly the true V-based catalyst.[2] In very recent studies we have gone on to show that the key to the catalyst evolution process, from virtually any V-based precatalyst tested, is the formation of a novel, autoxidation-product-initiated dioxygenase catalyst. In that reaction, initial DTBC autoxidation to 3,5-di-*tert*-butyl-1,2-benzoquinone also produces H_2O_2 which, in turn, autocatalytically results in the formation of catalytically active [VO(DBSQ)(DTBC)]$_2$.[3]

Scheme 1. Oxidative Cleavage of DTBC by Vanadium-Containing Polyoxometalate Precatalysts[a]
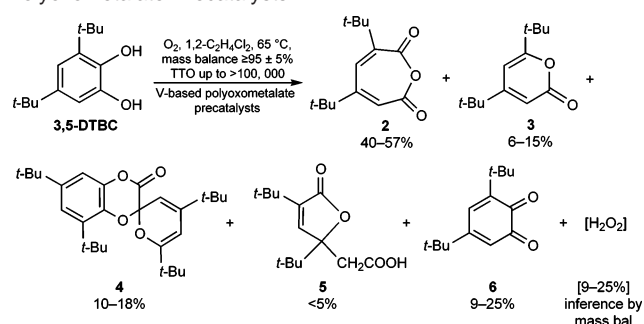
[a] The established products[1] are **2**, 3,5-di-*tert*-butyl-1-oxacyclohepta-3,5-diene-2,7-dione; **3**, 4,6-di-*tert*-butyl-*2H*-pyran-2-one; **4**, spiro[1,4-benzo-dioxin-2(*3H*),2'(*2H*)-pyran]-3-one, 4',6,6',8-tetrakis(1,1-dimethylethyl); **5**, 3,5-di-*tert*-butyl-5-(carboxymethyl)-2-furanone; and **6**, 3,5-di-*tert*-butyl-1,2-benzoquinone.

Herein we report kinetic studies, beginning with the [VO(DBSQ)(DTBC)]$_2$ dimer, (i) which show that this dimer is the catalyst resting state, (ii) which show that dissociation of the dimer to monomeric VO(DBSQ)(DTBC) is required for reaction with O_2, and (iii) which allow, along with insights from classic literature studies of other dioxygenases,[4,5] a mechanism of action

(1) Weiner, H.; Finke, R. G. *J. Am. Chem. Soc.* **1999**, *121*, 9831$-$9842.
(2) Yin, C.-X.; Finke, R. G. . *J. Am. Chem. Soc.* **2005**, *107*, 9003$-$9013.
(3) Yin, C.-X.; Sasaki, Y.; Finke, R. G. *Inorg. Chem.* **2005**, in press.

(4) Jang, H. G.; Cox, D. D.; Que, L., Jr. *J. Am. Chem. Soc.* **1991**, *113*, 9200$-$9204.
(5) (a) Winfield, C. J.; Al-Mahrizy, Z.; Gravestock, M.; Bugg, T. D. H. *Perkin 1* **2000**, 3277$-$3289. (b) Bugg, T. D. H.; Lin, G. *Chem. Commun.* **2001**, 941$-$952.

to be written for V-based DTBC dioxygenases. The results simplify and unify the previously disparate V-based dioxygenase literature. Moreover, since the catalytic lifetimes are without precedent in prior man-made or *proven* lifetime enzymatic dioxygenases (see footnote 27 in ref 1), the results are of fundamental significance in providing insight into man-made, highly catalytic, long-lived and mechanistically understood dioxygenase catalysts, the Holy Grail of oxidation catalysis.[6]

Experimental Section

Reagents. DTBC (Aldrich, 99%) was recrystallized three times using *n*-pentane (Fisher Scientific, 98%, pesticide grade) under argon (melting point 99–100 °C, lit. mp 96–99 °C) and stored in a Vacuum Atmosphere drybox (O_2 level ≤ 5 ppm). (NB: It is important to recrystallize the DTBC substrate ≥2 times to remove impurities like 3,5-di-*tert*-butylbenzoquinone, due to effects such as shown in Figure 2 in ref 3.) 1,4,7-Triazacyclononane (Strem, 97%) and 1,4,7-trimethyl-1,4,7-triazacyclononane (Strem, 97% min.) were stored in the drybox and used as received. HPLC-grade solvent (1,2-dichloroethane) was purchased from Aldrich and stored in the drybox; the above solvent was dried by standing for at least 48 h over ~5 vol % 3- or 4-Å molecular sieves which were preactivated by heating at 170 °C under vacuum for at least 12 h, then cooling under dry N_2 in the drybox. Anhydrous-grade toluene (Aldrich) was used as received and stored in the drybox.

Instrumentation. GC analyses were performed on a Hewlett-Packard (HP) 5890 Series II gas chromatograph equipped with an FID detector and an SPB-1 capillary column (30 m, 0.25 mm i.d.) with the following temperature program: initial temperature, 200 °C (initial time, 2 min); heating rate, 2 °C/min; final temperature, 240 °C (final time, 3 min); FID detector temperature, 250 °C; injector temperature, 250 °C. An injection volume of 1 μL was used. UV–visible spectra were obtained on an HP 8452A diode spectrophotometer in glass UV cells. Electron paramagnetic resonance (EPR) spectra were recorded on a Bruker EMX 200U EPR spectrometer. Quartz EPR tubes of 4-mm o.d. were used, and 2,2-diphenyl-1-picrylhydrazyl (DPPH) was used as the reference compound (g = 2.0037).

Preparation of Pierpont's Complex. [VO(DBSQ)(DTBC)]$_2$ was prepared and characterized by UV–visible, elemental analysis, and negative ion ESI-MS as previously detailed.[2]

O_2-Uptake Kinetic Experiments and Rate Law Determination. These experiments were carried out as detailed elsewhere[7] on a computer-interfaced O_2-pressure transducer apparatus which permits the collection of high-precision (≤±0.01 psig) pressure data at ≥1 data points per second. The reaction flask is a pressurized Fischer–Porter bottle attached via Swagelock quick-connects and flexible stainless steel tubing to both an oxygen tank and a pressure transducer (total volume 148 mL).[7] In the drybox, 400 ± 5 mg (1.8 mmol) of DTBC was weighed into a 22 mm × 175 mm Pyrex culture tube along with a $^5/_8$-in. × $^5/_{16}$-in. Teflon stir bar. Pierpont's catalyst [VO(DBSQ)(DTBC)]$_2$ (typically 2–8 mg, 1.8–7.2 mol) was weighed into a 5-mL glass vial and dissolved in a measured volume of 1,2-$C_2H_4Cl_2$ (1–3 mL). A predetermined fraction (ca. 1/10–1/3; 0.4–0.8 mol) of this stock solution was transferred into the culture tube via a 1-mL syringe. The culture tube was then placed inside the Fischer–Porter bottle, sealed, brought out of the drybox, placed in a temperature-controlled oil bath, and attached to the oxygen uptake apparatus via the quick-connects. Stirring was initiated and the solution was equilibrated in the oil bath (40 °C) under N_2 (from the drybox gas) for 25 min. The Fischer–Porter bottle was then purged 15 times with ~13 psig of O_2

(~1.7 atm), 15 s per purge, followed by equilibration for 1 min 15 s; 5 min total time elapsed before the pressure recordings were started. Note that the atmospheric pressure at the ca. 1-mile-high altitude of Fort Collins, Colorado, is around 632 Torr, or 0.83 atm. The reaction vessel was then pressurized to 13 ± 1 psig and t = 0 was set. The results are shown in Figures 1–4.

The O_2 rate vs catalyst concentration, gas-to-solution mass-transfer limitation plot is included in the Supporting Information as Figure S1. Those data, obtained at a stirring rate of 1200 rpm, indicate a clean first-order catalyst dependence up to ca. 0.1 mM, so O_2 mass-transfer limitations should not be a concern for the kinetic experiments leading to the reaction orders in substrate and O_2 which were performed at ca. 0.05 mM and a 1200 rpm stirring rate. In all cases, the raw kinetic data from the O_2-uptake kinetics obtained with the pressure transducer were corrected for the contribution of the solvent vapor pressure in the early part of the curves (i.e., after flushing with O_2 to start the reaction and prior to those curves coming to equilibrium). This correction was done exactly as detailed earlier[3] via the measurement of the solvent-vapor-pressure curve in an independent experiment. (An exemplary curve is provided in the Supporting Information as Figure S2, along with additional details of how the correction for the solvent vapor pressure was accomplished.[3]) The corrected, typically initially linear O_2 pressure–time plots (e.g., Figures 1, S3, and S4) were analyzed by linear regression of their initial linear portion to obtain initial rate data.

Reaction Rate of [VO(DBSQ)(DTBC)]$_2$ with O_2 As Estimated by UV–Visible Spectroscopy. The rate of reaction of [VO(DBSQ)(DTBC)]$_2$ plus O_2 was estimated by following the decay of the absorbance peak at 684 nm of [VO(DBSQ)(DTBC)]$_2$ (0.15 mol in 3 mL of 1,2-$C_2H_4Cl_2$, 0.05 mM) after O_2 was bubbled into the UV cell which had been prewarmed to ca. 40 °C. The initial rate of reaction, obtained from the first three data points over 20 min of reaction, is 1.9 h^{-1} (pseudo-first-order rate constant when assuming O_2 is in excess, $[O_2]_{solution}$ ≈ 5 mM[9] at 293.2 K, 0.8 atm O_2; the initial second-order rate constant is ca. 380 M^{-1} h^{-1} assuming a second-order rate law and using the $[O_2]_{solution}$ ≈ 5 mM).

Kinetic Curve-Fitting Using MacKinetics. For the equations in Scheme 2 of (in generalized form) A ⇌ 2B, B + O_2 → D + product, then 2D + 2DTBC → A, numerical integration curve-fitting via MacKinetics was employed. The oxygen pressure in psig was converted to soluble O_2 in M by setting up an oxygen reservoir to mimic the oxygen concentration in the solution following the calculation method first used by D. K. Lyon[8] along with literature O_2 solubility data (a Henry's constant of 15340 Pa m^3/mol at 293.2 K in 1,2-dichloroethane);[9] the resultant ($[O_2]_t - [O_2]_{final}$)[10] experimental data were then used in the fitting. To start, the chemical equations to be tested were written into MacKinetics along with the experimental data set. Next, a grid search was performed to fit the kinetic parameters to the experimental data. Specifically, the kinetic parameter search was performed first over a broad range of the parameters (10^{-10}–10^{10}) using the grid search command in MacKinetics. The grid search was then narrowed down to about half the previous range (e.g., if the first search gave k_1 = 0.01 and k_2 = 0.1 as the best fit in the range of 10^{-10}–10^{10}, then the second search was performed in the range of 10^{-7}–10^3 for k_1 and 10^{-6}–10^4 for k_2); the center of the new range was always set equal to the result from the last grid search as in the above examples. The search was deemed finished once a grid search was performed in a range no larger than 2 orders of magnitude. The curve-fit shown in

(6) Hill, C. L.; Weinstock, I. A. *Nature* **1997**, *388*, 332–333.

(7) Yin, C.-X.; Finke, R. G. Is It True Dioxygenase or Classic Autoxidation Catalysis? Re-Investigation of a Claimed Dioxygenase Catalyst Based On a Ru$_2$-Incorporated, Polyoxometalate Precatalyst. *Inorg. Chem.* **2005**, *44*, 4157–4188.

(8) Lyon, D. K. Ph.D. Dissertation, University of Oregon, Eugene, OR, 1990, p 252; see also pp 142–145.

(9) Lühring, P.; Schumpe, A. *J. Chem. Eng. Data* **1989**, *34*, 250–252.

(10) A result of using the zeroed, net $[O_2]$ concentration change which is necessary for the curve-fitting is that the different initial pressure is ignored; that is, $\Delta[O_2]$ is proportional only to the [DTBC] (total). Hence, the averaged rate constants reported in Scheme 2 are the result from curve-fitting just those eight sets of data obtained under the identical initial pressure (ca. 1.7 atm O_2).

Figure 1 (as well as Figures S3 and S4) is that obtained by performing a final integration, using the best set of kinetic parameters, and then co-plotting those data with the observed, experimental data. All other fits started with the parameters obtained from Figures 1, S3, and S4 and then performed a grid search over a range of 10^2 from those parameters.

Effect of the Addition of an O-Substituted Ligand to [VO-(DBSQ)(DTBC)]$_2$ As Monitored by EPR. A drop of DMSO (Mallinckrodt, spectrometric grade) was added to ca. 0.2 mM [VO(DBSQ)-(DTBC)]$_2$ in toluene. The nine-line EPR characteristic[2] of [VO(DBSQ)-(DTBC)]$_2$ ($g = 2.006$, $A_{51V} = 3.01$ G) changed to an asymmetric spectrum (a $g = 2.02$ broad peak, and $g = 2.002$ for five other sharp peaks, $A_{51V} = 6.35$ G) as shown in Figure S8 in the Supporting Information. A color change from blue to violet was also observed upon the addition of DMSO.

Results and Discussion

Rate Law of [VO(DBSQ)(DTBC)]$_2$-Catalyzed DTBC Dioxygenation: Support for This Dimer Being the Catalyst Resting State. Our previous paper[2] established Pierpont's complex [VO(DBSQ)(DTBC)]$_2$ as either a catalyst resting state or possibly an actual species within the main catalytic cycle. The application of one of the well-tested postulates of Halpern's "rules" (really guidelines) as detailed elsewhere,[11] that if you can isolate it (as one can with Pierpont's complex), it typically is not the catalyst (i.e., it is too stable to be a top catalytic intermediate, and is likely ≥1 step away from the true catalytic cycle), predicts that [VO(DBSQ)(DTBC)]$_2$ is mostly likely a catalyst resting state.

The kinetics when beginning with pre-made, isolated [VO-(DBSQ)(DTBC)]$_2$ were determined by following the oxygen pressure loss in order to confirm or refute this catalyst resting state hypothesis, that is, the hypothesis that this complex is directly connected to the catalytic cycle. In addition, we were interested in the following question: Does the intact dimer complex react directly with O$_2$, or must it first fragment to two monomers before entering the catalytic cycle? Note that the measured O$_2$ uptake is due to the *catalytic* reaction of DTBC with O$_2$ (i.e., and not the much smaller scale *stoichiometric* reaction of [VO(DBSQ)(DTBC)]$_2$ with O$_2$) since DTBC is present in a 750- to 9000-fold excess relative to [VO(DBSQ)-(DTBC)]$_2$. The details of how these experiments are done are also relevant to their correct interpretation: the mixture of [VO-(DBSQ)(DTBC)]$_2$ and DTBC was brought out of the drybox and flushed with O$_2$, followed by its necessary equilibration under that O$_2$ atmosphere for 5 min, before pressure readings were started, as described in more detail in the Experimental Section.

A representative O$_2$-uptake curve obtained for the reaction of [VO(DBSQ)(DTBC)]$_2$, DTBC, and O$_2$ is presented in Figure 1. Documentation that the linear plot in Figure 1 is representative is provided by the analogous kinetic curves under different DTBC or other conditions (Figures S3 and S4 of the Supporting Information). The linear nature of these curves proved to be a highly telling, albeit initially unexpected, diagnostic of the underlying mechanism. Note that at first glance (i) the initially linear concentration vs time plot would appear to imply a zero-order dependence on [O$_2$], so (ii) we checked to be sure that O$_2$ mass-transfer is not limiting the observed reaction rate. The

(11) Hagen, C. M.; Vieille-Petit, L.; Laurenczy, G.; Süss-Fink, G.; Finke, R. G. *Organometallics* **2005**, *24*, 1819−1831, see footnote 45 therein.
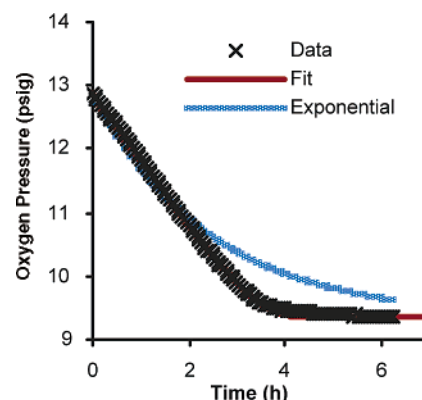
Figure 1. O$_2$-uptake curve of a representative kinetic run of DTBC plus [VO(DBSQ)(DTBC)]$_2$ and its curve-fit a là Scheme 2. Reaction conditions: 1.8 mmol of DTBC, 0.4 μmol of catalyst, 8 mL of 1,2-C$_2$H$_4$Cl$_2$, 40 °C, and 1.7 atm O$_2$. The initial rate obtained via a linear regression of the data obtained within the first hour is −1.0 psig/h (or −0.86 Torr/min). The fit (the solid line that fits the data so well it cannot be easily seen until at the bottom, right-hand end of the curve) is from numerical integration of the kinetic steps and mechanism in Scheme 2 accomplished via MacKinetics. The individual rate constants defined from the curve-fitting (and as defined in Scheme 2) are $k_3 \approx 600$ h^{-1}, $k_4 \approx 10^8$ M^{-1} h^{-1}, $k_5 \approx 3 \times 10^7$ M^{-1} h^{-1}, and $k_6 \approx 7 \times 10^9$ M^{-3} h^{-1}. The data and fit above are also compared to a first-order, exponential kinetic curve (pO$_2$(t) = pO$_{2,t=0}$ exp{$-k_{initial}$(t)}).
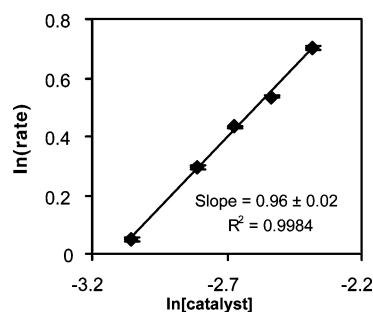
Figure 2. Logarithmic plot of the initial −d[O$_2$]/dt rate vs the concentration of [VO(DBSQ)(DTBC)]$_2$. Reaction conditions: 1.8 mmol of DTBC, 0.4−0.8 μmol of catalyst, 8 mL of 1,2-C$_2$H$_4$Cl$_2$, 40 °C, and 1.7 atm O$_2$. A clean first-order dependence of the initial rate on the initial concentration of [VO-(DBSQ)(DTBC)]$_2$ is apparent.

O$_2$ gas-to-solution mass-transfer rate for our apparatus, conditions, and stirring rate is ca. 24 Torr O$_2$/min·mM (the initial slope of the -d[O$_2$]/dt vs [[VO(DBSQ)(DTBC)]$_2$] plot shown in Figure S1 of the Supporting Information), so even at the highest concentration of [VO(DBSQ)(DTBC)]$_2$ studied in this work, any MTL effects should cancel within a ≤5% error (note also the linear slope in Figure 1 is ~0.86 Torr/min, below the 1.2 Torr O$_2$/min mass-transfer limit). In short, there must be some other explanation for the predominantly linear kinetic curves observed in place of the initially expected exponential curves due to a first-order consumption of O$_2$ (vide infra).

A successful solution to this kinetic puzzle came from the determination of the rate law by the initial rate method, some reflective thinking after being stumped for a bit by the linear kinetics, plus the use of MacKinetics numerical integration kinetic modeling. The initial rates were determined from the initial slope of the linear portion of the O$_2$-uptake curves. A logarithmic plot of the initial −d[O$_2$]/dt vs the [[VO(DBSQ)-(DTBC)]$_2$]$_{initial}$ is shown in Figure 2 and indicates a clean first-order dependence on [VO(DBSQ)(DTBC)]$_2$. A plot showing a zero-order dependence on the substrate [DTBC]$_{initial}$, as one
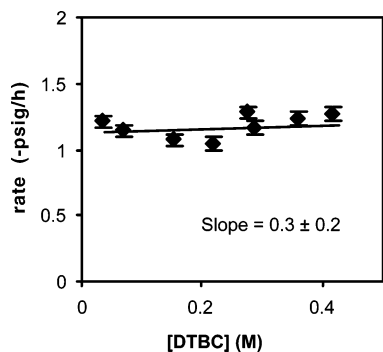
Figure 3. Plot of the initial rate vs substrate concentration. Reaction conditions: 0.3−3.6 mmol of DTBC, 0.4 μmol of catalyst, 8 mL of 1,2-$C_2H_4Cl_2$, 40 °C, and 1.7 atm O_2. The ±0.2 error bar in the figure is at 1σ, so that a zero-order dependence on DTBC is apparent even at 2σ error bars (0.3 ± 0.4).
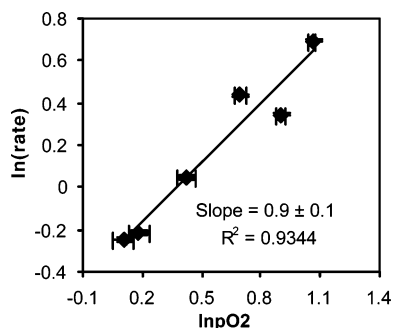
Figure 4. Logarithmic plot of the initial rate vs substrate pO_2 (in atm). Reaction conditions: 1.8 mmol of DTBC, 0.4 μmol of catalyst, 8 mL of 1,2-$C_2H_4Cl_2$, 40 °C, and 1.1−2.9 atm O_2. A first-order dependence on O_2 is apparent.

might have predicted for the DTBC-saturated complex, [VO-(DBSQ)(DTBC)]₂, is shown in Figure 3. Importantly, a *first-order rather than a zero-order dependence on $pO_{2,initial}$* is demonstrated in Figure 4. The experimentally determined rate law for catalyst, DTBC, and O_2 is, then, the following (where it is understood that initial rates and concentration subscripts apply to each term):

$$-\frac{d[O_2]}{dt} = k_{obs}[DTBC]^0([VO(DBSQ)(DTBC)]_2)^1[O_2]^1$$

Things began to make sense, and the most probable mechanism of action began to unfold, at this point. The first insight is that this rate law *is just that expected for Pierpont's catalyst, [VO(DBSQ)(DTBC)]₂, being directly connected to the catalytic cycle*. The lack of a DTBC dependence is also as expected: [VO(DBSQ)(DTBC)]₂ does not need more DTBC, but does need O_2, as confirmed by the zero- and first-order dependencies, respectively, on these components of the observed stoichiometry, Scheme 1 (vide supra). The crucial and novel identification, in our prior paper,[2] of [V^V(O)(DBSQ)(DTBC)]₂ as directly connected to the catalytic cycle is, therefore, fully supported and further fortified by the kinetic studies and observed rate law obtained as part of this study.

Given the observed first-order pO_2 dependence (plus the zero-order DTBC dependence), the kinetic curve in Figure 1 should be *exponential*—if one also assumes a constant catalyst concentration. However, the exponential curve co-plotted in Figure 1 shows that the observed curve is clearly *not* exponential; instead it is linear over a substantial part, typically ca. 40−

70%, of the catalytic reaction, as shown in Figure 1 (and as also documented in Figures S3 and S4 of the Supporting Information).

After some reflection, we reasoned that an exponentially decreasing rate due to the consumption of pO_2 (i.e., its first-order dependence) is being compensated by an effectively increasing (and thus rate-increasing) concentration of another component in the catalytic cycle. Given the rate law observed, *the only option for that other increasing component is the vanadium catalyst*. We further reasoned that, therefore, it is highly probable that the added [VO(DBSQ)(DTBC)]₂ is acting as a catalyst resting state and is supplying a second V species that is more active and is the true catalyst which reacts directly with O_2 within the main catalytic cycle.

A hypothesis for this hidden V species quickly became apparent, and the mechanism continued to unfold: the dimer, [VO(DBSQ)(DTBC)]₂, is very likely (i) fragmenting to two monomers, 2VO(DBSQ)(DTBC), and (ii) that fragmentation is very likely reversible (to allow for a subsequent rate-determining reaction with O_2, as needed to account for the first-order pO_2 dependence). It also seems necessary that (iii) the overall rate of formation of the active monomer and the rate of the DTBC oxygenation in the catalytic cycle must be occurring at comparable rates (i.e., when one begins with [VO(DBSQ)-(DTBC)]₂) so that an increasing catalyst concentration with its rate-increasing effect can occur on the same time scale as the rate-decreasing O_2 consumption shown in Figures 1, S3, and S4.

Scheme 2. A Minimum-Step, Kinetic Mchanism Which Fits theObserved, Linear Kinetic Data in Figures 1, S3, andS4 (Plus Five Additional Sets of Data, Eight Data Sets Total)[a]
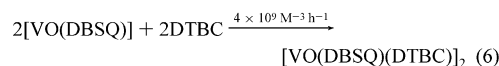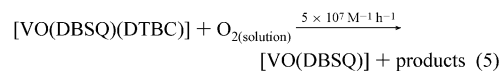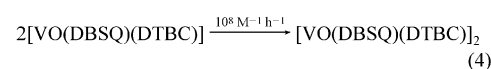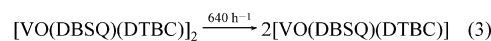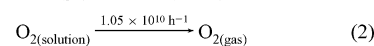
[a] Individual steps are shown as they must be entered into MacKinetics (i.e., steps 1 and 2 are just the O_2 gas-to-solution equilibrium, while steps 3 and 4 are the separate steps of the dimer-to-monomer equilibrium). The rate constants for steps 1 and 2 are meaningless as they were set at high, artificial values so as to provide a fast prior equilibrium; however, their ratio was set to faithfully reflect the known solubility of O_2 in 1,2-$C_2H_4Cl_2$ at 20 °C and 1.7 atm O_2.[9] The rate constants shown for steps 3−6 are those found by the MacKinetics curve-fitting of the experimental data.

The particular kinetic scheme we then wrote and tested via MacKinetics numerical integration is shown in Scheme 2. Key components of the kinetic mechanism shown in Scheme 2 are (i) a fast, reversible non-MTL O_2 gas-to-solution pre-equilibrium (as our MTL studies support), one in which the rate constants are artificially set as very high (i.e., to mimic a fast prior equilibrium), but where the ratio of rate constants correctly

reflects the O_2 solubility in dichloroethane[9] at 20 °C all as done previously[8] (i.e., an O_2 reservoir[8] was constructed); (ii) a reversible fragmentation of the dimer $[VO(DBSQ)(DTBC)]_2$ to two monomers, $2VO(DBSQ)(DTBC)$; (iii) the reaction of each monomer with O_2 and conversion into $VO(DBSQ)$ plus organic product, and then importantly (iv) a fast step regenerating the dimer, $[VO(DBSQ)(DTBC)]_2$.

Controls were done on the curve-fitting en route to arriving at the steps shown in Scheme 2: if step 6 is replaced with the monomer-forming step, $[VO(DBSQ)] + DTBC \rightarrow [VO(DBSQ)(DTBC)]$, then a poor fit is obtained, as shown in Figure S5 in the Supporting Information. In addition, a mechanism in which intact $[VO(DBSQ)(DTBC)]_2$ is directly part of the catalytic cycle (Scheme S1 of the Supporting Information) also cannot fit the observed data, as illustrated in Figure S6 of the Supporting Information.

The stoichiometry coefficients of *two* $[VO(DBSQ)]$ plus *two* DTBC in step 6 of Scheme 2 merit some comment: since their sum is greater than three, this reaction cannot be an elementary step (i.e., it must be pseudoelementary[12,13]). Hence, controls on the curve-fitting were performed by varying the coefficients: to one $[VO(DBSQ)]$ and one DTBC to form $0.5[VO(DBSQ)(DTBC)]_2$ (an excellent fit resulted with an essentially unchanged $k_6 = 1.1 \times 10^{10}$ M^{-2} h^{-1}) as well as two $[VO(DBSQ)]$ and one DTBC (again an excellent fit, with the same rate constant within experimental error, $k_6 = 10^9$ M^{-2} h^{-1}). An attempted fit with one $[VO(DBSQ)]$ and two DTBC in step 6 did not converge, however. The end result of these curve-fitting controls is that they support the formulation of step 6 as shown in Scheme 2 of a net reaction of two $[VO(DBSQ)]$ reacting with two DTBC.

In response to an insightful reviewer's question and suggestion, an alternative way to write eqs 5 and 6, which avoids a V(III) product, but which yields the same rate constants for these steps and which is consistent with Scheme 3 (vide infra), is as follows:

$$[V^VO(DBSQ)(DTBC)] + O_2 \rightarrow [V^VO(DBSQ)(O_2DTBC)] \tag{5}$$

$$2[V^VO(DBSQ)(O_2DTBC)] + 2H_2DTBC \rightarrow [V^VO(DBSQ)(DTBC)]_2 + 2H_2(O_2DTBC) \tag{6}$$
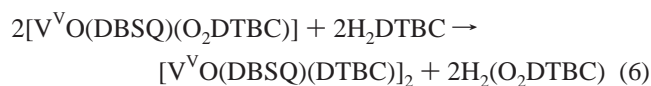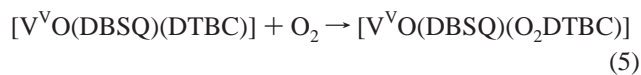
where O_2DTBC^{2-} is meant to indicate the conjugate base of the oxidation product. Since the products of steps 5 and 6 are after the rate-determining step (step 5), we have no direct information on which detailed versions of steps 5 and 6 are correct.

The accuracy of the resultant rate constants in Scheme 2 also merits comment; our experience is that factors of 2- to 10-fold (or more) can result from such fitting of kinetic data to four unknowns, depending on the particulars of the kinetic scheme, the amount and quality of the data (which are high for the

(12) (a) Original work using the pseudoelementary step concept as a kinetic tool in understanding oscillatory reactions: (a) Field, R. J.; Noyes, R. M. *Acc. Chem. Res.* **1977**, *10*, 214−221. (b) Noyes, R. M.; Field, R. J. *Acc. Chem. Res.* **1977**, *10*, 273−280. (c) Noyes, R. M.; Furrow, S. D. *J. Am. Chem. Soc.* **1982**, *104*, 45−48.
(13) We have further developed the pseudoelementary step concept in our mechanistic work on a ≫300-step self-assembly reaction forming Ir(0)$_{\sim300}$ nanoclusters: (a) Watzky, M. A.; Finke, R. G. *J. Am. Chem. Soc.* **1997**, *119*, 10382−10400. (b) Widegren, J. A.; Aiken, J. D., III; Özkar, S.; Finke, R. G. *Chem. Mater.* **2001**, *13*, 312−324.

Figure 5. Calculated $[VO(DBSQ)(DTBC)]$ monomer concentration vs time curve obtained using the chemical equations and rate constants shown in Scheme 2. Note that the maximum concentration of the active monomer builds up to about 0.017 mM, that is, to ca. one-third of the initial concentration of the initial dimeric catalyst resting state, $[VO(DBSQ)(DTBC)]_2$, concentration.

present pressure-transducer-obtained data), and other factors. Consistent with this, the rate constants for the data in Figures S3 and S4 in comparison to that for Figure 1 do show values that differ by factors of 2- to 7-fold. Hence, the rate constants reported in Scheme 2 are the averages of Figures 1, S3, and S4, and five other (eight total) data sets obtained under a range of catalyst concentrations (0.04−0.09 mM) and DTBC concentrations (0.15−0.42 M). In addition and as discussed next, an experiment was designed to independently test the reliability of the equilibrium and rate constants listed for the first five steps in Scheme 2.

UV−Visible Monitoring of the Reaction of the Initial Rate of $[VO(DBSQ)(DTBC)]_2$ Plus O_2. Since step 5 in the kinetic mechanism in Scheme 2 is the rate-determining step following two fast prior equilibria, Scheme 2 and its rate constants predict that the observed rate constant for the summation of the first five steps will look like the following (obtained using the rate constant definitions and values contained in Scheme 2 as well as the steady-state assumption on the dissolved O_2 and monomer intermediates): $k_{obs} = K_{1,2}K_{3,4}k_5$, where the equilibrium constant for steps 1 and 2, $K_{1,2}$, is ∼10^{-2}, that for steps 3 and 4, $K_{3,4}$, is ∼7×10^{-6} M, and $k_5 \approx 5 \times 10^7$ M^{-1} h^{-1}. Hence, the prediction from Scheme 2 is that $k_{obs} \approx 3.5$ h^{-1}.

Experimentally, it was found that the reaction of $[VO(DBSQ)(DTBC)]_2$ with O_2, by following the UV-absorbance decay of $[VO(DBSQ)(DTBC)]_2$ at 684 nm and while at 40 °C and 0.8 atm O_2, pleasingly yields a very close initial-rate-determined $k_{obs} = 1.9$ h^{-1} that is within a factor of ∼2 of the predicted 3.5 h^{-1}. This independent result provides both an idea of the precision of the rate constants in Scheme 2 as well as a general confirmation of the first five steps in Scheme 2, the data fitting procedure, and the resultant rate constants. This result also confirms that steps 1−2 and 3−4 represent two fast prior equilibria, so the steady-state assumption on the dissolved O_2 and monomer intermediate used to obtain the $k_{obs} = K_{1,2}K_{3,4}k_5$ equality is also supported.

Use of MacKinetics To Better Understand the Linear Kinetic Curves. Next, we used that numerical kinetic model in Scheme 2 plus MacKinetics in their powerful, predictive way. First, we generated the calculated monomer concentration vs time curve shown in Figure 5. Note that it does indeed show

the expected (vide infra) increasing concentration vs time needed to rationalize why the kinetic curves are linear: the rate-increasing effect of increasing monomer concentration is convoluted experimentally with the exponential rate decrease due to the first-order loss of O_2; the result is an apparently linear kinetic curve (e.g., Figures 1, S3, and S4). Second, we generated the predicted kinetic curves as a function of the initial [VO-(DBSQ)(DTBC)]$_2$ concentration, determined the initial rates from those computed data, and then plotted those initial rates vs the initial concentrations to be sure that the rate law determined from the initial rates is consistent with the kinetic model and rate constants in Scheme 2. The result, shown in Figure S7 of the Supporting Information (which basically mirrors Figure 2, vide supra), again shows that the kinetic model in Scheme 2 *is fully consistent with the measured rate law obtained using initial rate methods*.

Noteworthy here is that the mechanism in Scheme 2 is a rare (and possibly the first) experimental example of the generalized kinetic scheme A $\rightleftharpoons$ 2B, B + C $\rightarrow$ D + product, then 2D + 2E $\rightarrow$ A. As such, it is of interest to study its general properties further by numerical integration simulations as a function of the concentrations of each variable and the four rate constants involved. These simulations are being carried out as a separate study.[14]

A Proposed Mechanism Consistent with the Kinetics, the Catechol Dioxygense Literature, and Employing [VO(DB-SQ)(DTBC)]$_2$ as the Catalyst Resting State. A proposed system for the active vanadium catechol dioxygenase mechanism is provided in Scheme 3. This mechanism is of course consistent with our kinetic studies, but then it also incorporates key features from the literature of the Fe-based catechol dioxygenases, notably the substrate activation mechanism proposed by Que and co-workers,[4] the M—OO—C(catechol) species characterized by Bianchini and co-workers,[16] as well as a common branching intermediate for intradiol vs extradiol cleavage pathways as detailed by Bugg and co-workers.[5]

Based on our earlier finding and the kinetic studies herein, Pierpont's complex is unequivocally identified as *the catalyst resting state*. In step 1 in Scheme 3, the [VO(DBSQ)(DTBC)]$_2$ reversibly fragments in even weakly coordinating solvent to form 2 equiv of monomer. Five lines of evidence support this step: (1) the kinetic studies and MacKinetics curve-fitting; and (2) an experiment in which even a drop of DMSO added to [VO(DBSQ)(DTBC)]$_2$ in toluene changes the signature nine-

line EPR spectrum to the asymmetric spectrum as shown in Figure S8 along with a dramatic color change from blue to violet. (A reviewer commented that oxo-transfer to DMSO could be involved in this reaction; we agree, and thank the reviewer for noting this possibility.) Additional evidence for a facile dimer-to-monomer equilibrium is the following: (3) Pierpont's demonstration of a facile dimer–monomer equilibrium for related Mo complexes;[17] (4) literature structural studies showing that vanadium compounds with coordination numbers of 5 or 6 are the most common so that only the monomer is expected to react quickly with O_2 (formally seven-coordinate compounds typically contain a cyclic peroxo component occupying two adjacent sites;[18] we thank Prof. Cortland Pierpont at the University of Colorado for this point); and (5) the mechanism in which intact [VO(DBSQ)(DTBC)]$_2$ persists inside the catalytic cycle with, for example, only one vanadium being active, Scheme S1 of the Supporting Information (i.e., similar to enzymatic half-site reactivity[19]), *cannot* fit the observed kinetic data (vide supra) and also seems sterically prohibitive with no clear chemical advantage, at least not that we have been able to discern.

In step 2, O_2 binds to either the semiquinone[20] or the more nucleophilic catecholate ligand, as Bianchini[16] and Pierpont advocate,[21] in the [VO(DBSQ)(DTBC)] monomer as an individually fast *but still rate-determining* step in the catalytic cycle, consistent with the experimental kinetics. Step 2 is fast but rate-determining since the reverse of step 1 is faster than step 2 (which is also fairly fast). Note that the fact that step 2 is rate-determining means that the species after this and until the catalyst resting state do not build up to significant concentrations and thus are not expected to be amenable to typical spectroscopic characterization. This means that the species after step 2 in Scheme 3 must rely on steps that have to be present in order to account for the observed products plus literature precedent for the details of those steps.

(14) Morris, A. M.; Yin, C.-X.; Finke, R. G. Unpublished results and experiments in progress.

(15) The terminal V—O oxo is represented in Scheme 3 as a V≡O simply out of convenience; it certainly has some triple bond character based on Pierpont's structural studies. More specifically, the V—O bonds in [VO-(DBSQ)(DTBC)]$_2$ (bond length 1.581(4) Å[15a]) looks like a triple bond[15b,c] in comparison to the V=O bond length of 1.616(4) Å in the VO(catecho-late)$_2^{2-}$ ion. However, competing π bonding from the good π donor catecholate ligands is also present and needs to be a part of any discussion of the best descriptions of the V—O bonds. Two of the V—O(catecholate) bond lengths in [VO(DBSQ)(DTBC)]$_2$ are quite short, 1.827(4) Å, in comparison to V—O(semiquinone) bond length of 1.975–1.987 Å, showing the variable interactions present between V and catecholate or semiquinone oxygen atoms. (a) Cass, M. E.; Green, D. L.; Buchanan, R. M.; Pierpont, C. G. *J. Am. Chem. Soc.* **1983**, *105*, 2680–2686. (b) We thank Professor C. G. Pierpont for a discussion and his insights on this point. (c) Nugent, W. A.; Mayer, J. M. *Metal–Ligand Multiple Bonds*; John Wiley & Sons: New York, 1988; pp 33–36. (d) The classic Rappé–Goddard importance of a spectator oxo ligand also merits mention with respect to Scheme 3: Rappé, A. K.; Goddard, W. A., III. *J. Am. Chem. Soc.* **1982**, *104*, 3287–3294.

(16) Barbaro, P.; Bianchini, C.; Linn, K.; Mealli, C.; Meli, A.; Vizza, F. *Inorg. Chim. Acta* **1992**, *198–200*, 31–56.

(17) (a) A Mo analogue, [Mo^{VI}O(DTBC)$_2$]$_2$, dissociates into monomer in coordinating solvent as demonstrated by NMR: Buchanan, R. M.; Pierpont, C. G. *Inorg. Chem.* **1979**, *18*, 1616–1620. (b) The tetramer (chiral square) [Mo^{IV}(μ-O)(3,6-DTBC)$_2$]$_4$ also dissociates into monomer upon ligand addition: Liu, C.-M.; Nordlander, E.; Schmeh, D.; Shoemaker, R.; Pierpont, C. G. *Inorg. Chem.* **2004**, *43*, 2114–2124.

(18) (a) Nugent, W. A.; Mayer, J. M. *Metal–Ligand Multiple Bonds*; John Wiley & Sons: New York, 1988; pp 159–162. (b) The Cambridge Structural Database (version 5.26 Nov 2004) via Conquest (version 1.7) software.

(19) Enzymic half-site reactivity is observed in proteins composed of *n* identical subunits but which react with a substrate or an inhibitor with only *n*/2 subunits saturated with that ligand. Binding of the ligand to one site typically induces a conformational change of the second binding site, thereby rendering the second site inactive. (a) Levitzki, A.; Stallcup, W. B.; Koshland, D. E., Jr. *Biochemistry* **1971**, *10*, 3371–3378. (b) Seydoux, F.; Malhotra, O. P.; Bernhard, S. A. *CRC Crit. Rev. Biochem.* **1974**, *2*, 227–257.

(20) The proposed C_2 (instead of C_1) site of attachment of O_2 to the 3,5-di-*tert*-butylsemiquinone ligand in [VO(DBSQ)(DTBC)]$_2$ shown in Scheme 3 is consistent with the major product being 4,6-di-*tert*-butyl-*2H*-pyran-2-one, rather than its isomer, 3,5-di-*tert*-butyl-*2H*-pyran-2-one. We note, however, that both C_1 and C_2 binding of O_2 can give the intradiol product, **2**, a detail not included in Scheme 3 only to keep if from being too cluttered. Of interest here is that computed net *cationic* charges at C_1 (0.44) versus C_2 (0.42) have been reported for the cationic [Co^{III}(di-*tert*-butylcatecholato)-(MeC(CH$_2$PPh$_2$)$_3$)]$^+$.[20a] (a) Bencini, A.; Bill, E.; Mariotti, F.; Totti, F.; Scozzafava, A.; Vargas, A. *Inorg. Chem.* **2000**, *39*, 1418–1425. (b) Mechanisms with O_2 bound to the C_2 site of DTBC are commonly proposed in the literature: Cox, D. D.; Que, L., Jr. *J. Am. Chem. Soc.* **1988**, *110*, 8085–8092. (c) Viswanathan, R.; Palaniandavar, M. *J. Chem. Soc., Dalton Trans.* **1995**, 1259–1266. (d) Funabiki, T.; Yamazaki, T. *J. Mol. Catal. A: Chem.* **1999**, *150*, 37–47. (e) Yamahara, R.; Ogo, S.; Watanabe, Y.; Funabiki, T.; Jitsukawa, K.; Masuda, H.; Einaga, H. *Inorg. Chim. Acta* **2000**, *300–302*, 587–596.

(21) The mechanistic issues of the site and timing of the O_2 plus bound catecholate benefited from several discussions with Prof. C. Pierpont; it is our pleasure to acknowledge and thank him for those insightful discussions.

Scheme 3. Proposed, Minimal ("Occam's Razor") Mechanism of Vanadium-Based DTBC Dioxygenases Based on the Evidence Provided as Well as Literature Evidence[4,5,16] for Steps 3 and 4[15,a]

t-Bu

t-Bu

t-Bu

t-Bu

t-Bu

t-Bu

Catalyst Resting State

1

2

t-Bu   t-Bu

t-Bu   t-Bu

2

2O$_2$

2DTBC

5

2DTBC

t-Bu   O–O$^\bullet$ t-Bu

2

t-Bu   t-Bu

3

t-Bu

t-Bu

t-Bu

4b
alkenyl
migration

t-Bu O–O

2

b
a

t-Bu

V^V(O)(DBSQ)

t-Bu

O$^-$

V^V(O)(DBSQ)

EXTRADIOL

t-Bu

OH

OH

t-Bu

t-Bu

t-Bu

O

O$^-$

V^V(O)(DBSQ)

4a
acyl
migration

t-Bu

COOH

t-Bu

COOH

INTRADIOL
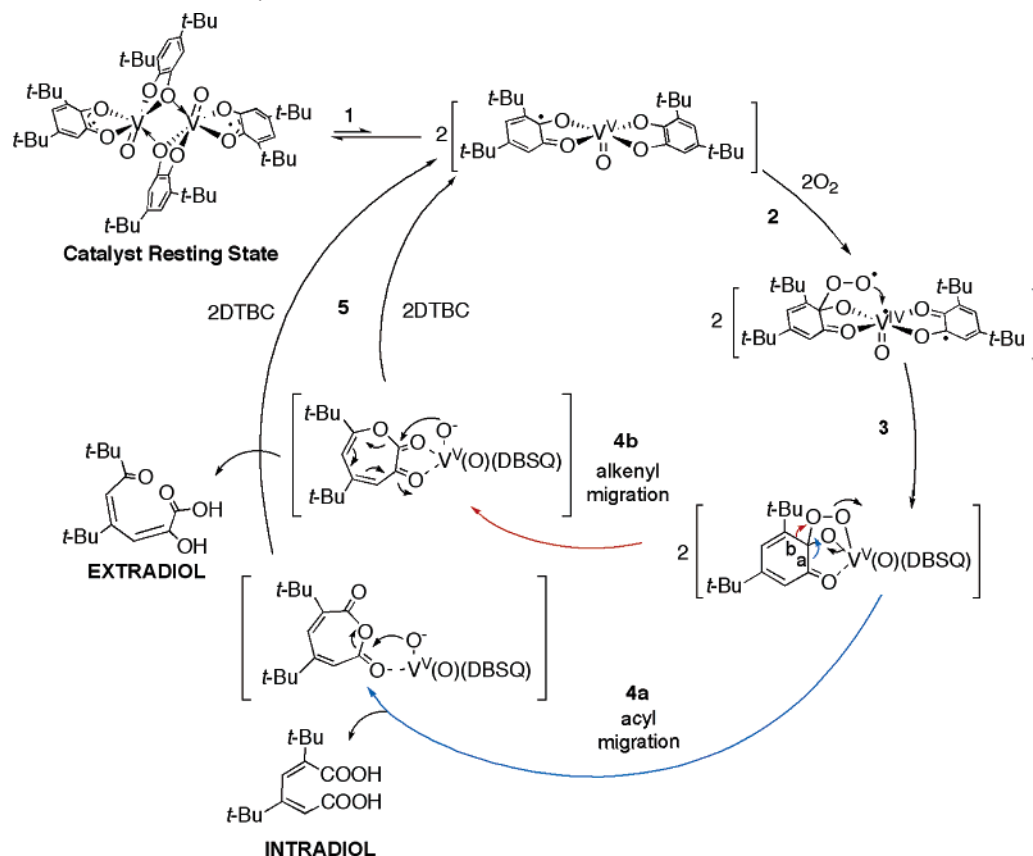
[a] The details of step 2 are less clear, however; both an O$_2$ diradical plus semiquinone spin-pairing mechanism (basically as shown above) and an electrophilic O$_2$ plus nucleophilic DTBC^{2-} mechanism are possible. See Scheme S2 of the Supporting Information as well as the text which follows for additional information and discussion.

The redox noninnocent[22] DTBC ligand (i.e., its catecholate/ V(V) as well as semiquinone/V(IV) forms) and the presence of both catechol and semiquinone in the active monomer introduce an at present unsolved mechanistic ambiguity—both here and in the general dioxygenase literature—as to which ligand form reacts initially with O$_2$. Noteworthy in this regard is Bianchini's classic study in which he considers three possible steps for the initial step leading to the metal—OO—C(catecholate) species: (i) the classic spin-pairng model, in which a O$_2$ diradical initially attacks a semiquinone radical; (ii) O$_2$ initial attack at the metal; or (iii) his preferred step, at least for Ir and Rh complexes, in which the more nucleophilic catecholate attacks *electrophilic* O$_2$, a step he notes is consistent with the metal-centered HOMO and ligand-centered LUMO. The mechanism shown above is basically the spin-pairing model (the facile reaction of the O$_2$ diradical and the semiquinone radical anion), followed by electron transfer from DTBC^{2-} to V^V to make DBSQ$^{-\bullet}$ and V^{IV} (i.e., valence tautomerism). The alternative possibility, which can be labeled the semiquinone spectator mechanism for step 2 in Scheme 3, is provided in Scheme S2 of the Supporting Information. Keys in that mechanism are nucleophilic attack of bound DTBC^{2-} on electrophilic O$_2$, with the vanadium remaining as V^V throughout the process. It would seem to us

that this latter mechanism might be disfavored due to the more substantial Marcus-type intrinsic barriers (at C and O$_2$; see the additional discussion in the Supporting Information). However, it is not possible to distinguish these mechanisms at the present time, so the ambiguity regarding the details of step 2 is the greatest uncertainty in Scheme 3 in our opinion.

A subsequent V—OO bond formation step is required in order to eventually obtain the O—O bond cleavage step required to account for the observed products; this step is written in Scheme 3 by analogy to the postulated mechanisms of enzymatic dioxygenases and their models. The presence of *two* catecholate/ semiquinone ligands on *one* vanadium is a noteworthy feature of the active monomer derived from Pierpont's dimeric catalyst resting state. Specifically, the presence of two DTBC ligands appears to prevent a dioxo V(O)$_2$ moiety from forming, a structural feature that in turn avoids a transient trioxo V(O)$_3$ moiety that would have been a violation of Lipscomb's rule[23]— and, therefore, presumably of too high energy to permit efficient catalysis. The presence of a spectator terminal oxo ligand[15d] in the catalyst, with its competing π-bonding effects, in Scheme 3 is also noteworthy.

The subsequent steps 3—4 have been written by analogy to the Fe catechol dioxygenase mechanism,[24] wherein a common

(22) (a) Jorgensen, C. K. *Absorption Spectra and Chemical Bonding in Complexes*; Pergamon Press: Oxford, 1962. (b) Collman, J. P.; Hegedus, L. S.; Norton, J. R.; Finke, R. G. *Principles and Applications of Organotransition Metal Chemistry*; University Science Books: Mill Valley, CA, 1987; pp 192—197.

(23) Pope, M. T. *Heteropoly and Isopoly Oxometalates*; Springer-Verlag: New York, 1983; pp 18—19.
(24) (a) Que, L., Jr.; Ho, R. Y. N. *Chem. Rev.* **1996**, *96*, 2607—2624. (b) Costas, M.; Mehn, M. P.; Jensen, M. P.; Que, L., Jr. *Chem. Rev.* **2004**, *104*, 939—986.

intermediate branches into intradiol cleavage product or extradiol cleavage product depending on migration of an acyl group (step 4a) or an alkenyl group (step 4b).[25] The product release in steps 4–5 is written as DTBC-dependent, but after the rate-determining step and fast, consistent with the zero-order dependence seen on DTBC as well as the finding that this step is fast based on the MacKinetics numerical integration kinetic model. (Recall here the earlier discussion about steps 5 and 6 *in the numerical integration model* and the two possibilities discussed there about precisely how to write these post-rate-determining steps.) The relative rate constants for the reverse of step 1 vs that of step 2 teach that active VO(DBSQ)(DTBC) monomer catalyst returns to the dimeric [VO(DBSQ)(DTBC)]$_2$ catalyst resting state about two times for every one time it reacts with O$_2$ to undergo another catalytic cycle.

Of course, like all new mechanisms, Scheme 3 is offered— and should be viewed—as a specific hypothesis requiring further testing and attempts to refine or refute its overall features as well as its intimate steps. That said, key features of Scheme 3 which are expected to stand the test of time include the identification of [VO(DBSQ)(DTBC)]$_2$ as the catalyst resting state, its fragmentation to monomer to enter the catalytic cycle, and the reaction of that monomer with O$_2$.

Effect of Added Tridentate Ligands on Catechol Oxidative Cleavage Activity. Based on the mechanism in Scheme 3, a prediction is that added ligands are not likely to have a beneficial effect, even if they are multidentate ligands that are useful in other dioxygenase catalysts.[26] In fact, the in situ addition of tridentate ligands such as 1,4,7-triazacyclononane (TACN) to a [VO(DBSQ)(DTBC)]$_2$-catalyzed DTBC oxygenation solution suppresses almost completely the dioxygenase reaction (the yield of intradiol product **2** decreased from ~40% to <0.2%), while the undesired autoxidation pathway increases (the yield of product **6** increased from ~18% to 41%).[27] This experiment both (i) confirms the importance of having two DTBC ligands in the active catalyst and (ii) argues that the design of kinetically highly active but more selective catechol oxygenation catalysts based on vanadium will be challenging.

Summary and Conclusions

The main findings from this study can be summarized as follows:

(i) Pierpont's structurally characterized complex [VO(DBSQ)-(DTBC)]$_2$ has been shown to be directly connected to the catalytic cycle, serving as a catalyst resting state.

(ii) Reversible fragmentation of Pierpont's dimer to active monomer, which then reacts with O$_2$ in a rate-determining step, is the second key finding of the present kinetic and mechanistic studies.

(iii) A proposed mechanism of action has been forwarded (Scheme 3) that is supported by the identity of the catalyst resting state and the kinetics from that resting state—the most a catalytic mechanistic chemist can ever ask for!—as well as a sizable amount of relevant literature.[2,24] The mechanism in Scheme 3 is offered as a working hypothesis that should be viewed as such and which can, and should, be used to guide future research; the details of the O$_2$ plus substrate addition step (step 2 in Scheme 3) especially require further investigation. The mechanism in Scheme 3 is, nevertheless, a welcome addition to a literature in which *mechanistic knowledge was previously nonexistent for any man-made catalyst that is as highly catalytic and long-lived as the present system (i.e., 30 000–100 000 TTOs).*

(iv) The mechanism in Scheme 3 also provides general support for the broader applicability of the mechanistic insights from the laboratories of Que,[4,24] Funabiki,[28] Bugg,[5] and others that went into the construction of the post-rate-determining steps 3–5 in Scheme 3. Restated, the way that the precedent in the literature from the seminal contributions of the above authors fits naturally into Scheme 3 provides support for the broader generality of the substrate coordination, C–OO–V formation, Criegee rearrangement, and other steps commonly seen in literature dixoxygenase mechanisms.[4,5,24]

(v) Point iv then, in turn, supports the probably greater generality of important mechanistic insights from the literature[24] and in Scheme 3, such as the observation that a major difference between dioxygenase and monooxygenases is that the former avoid O–O bond-cleavage activation of O$_2$. That is, Fe(II) extradiol[24] and Fe(III) intradiol,[24] as well as the present V(V/IV) combined intra- and extradiol dioxygenase, avoid O–O bond cleavage until *after* a substrate C–O–O bond has been made.[24,29] Hence, easier dioxygenations use a substrate's prior coordination as a key to their catalysis; more difficult substrates (e.g., unactivated alkanes) require O$_2$ activation with 2e$^-$ and 2H$^+$ to species such as Fe=O that can then do these harder activations. This in turn implies that it will be difficult to develop true dioxygenases for RH and other difficult substrates, a conclusion Sen has also reached.[30]

The above conclusions are, however, not meant to imply that additional mechanistic work is not possible nor needed. Further tests of the mechanism in Scheme 3 are possible and thus need to be performed along with studies testing if Scheme 3 extends in a general way to other systems such as molybdenum.[17] Indeed, it is likely that the area of man-made, highly active, long-lived dioxygenase catalysts supported by kinetic studies leading to mechanistic understanding is just beginning.

(25) The mechanism in Scheme 3 contains a testable ^{18}O$_2$ labeling prediction that will reveal whether O-scrambling occurs with the initial "spectator oxo" present in the catalyst, an experiment which can, then, be compared to literature precedent [(a) White, L. S.; Nilsson, P. V.; Pignolet, L. H.; Que, L., Jr. *J. Am. Chem. Soc.* **1984**, *106*, 8312–8313. (b) Funabiki, T.; Mizoguchi, A.; Sugimoto, T.; Tada, S.; Mitsuji, T.; Sakamoto, H.; Yoshida, S. *J. Am. Chem. Soc.* **1986**, *108*, 2921–2932.] This experiment is under investigation.

(26) (a) Dei, A.; Gatteschi, D.; Pardi, L. *Inorg. Chem.* **1993**, *32*, 1389–1395. (b) Jo, D.-H.; Que, L., Jr. *Angew. Chem., Int. Ed.* **2000**, *39*, 4284–4287. (c) Lin, G.; Reid, G.; Bugg, T. D. H. *J. Am. Chem. Soc.* **2001**, *123*, 5030–5039.

(27) The use of another tridentate ligand, 1,4,7-trimethyl-1,4,7-triazacyclononane (Me$_3$-TACN), gives the same results: the addition of either a stoichiometric or an excess amount of Me$_3$-TACN (310 equiv) vs the precatalyst (*n*-Bu$_4$N)$_7$-SiW$_9$V$_3$O$_{40}$-catalyzed DTBC oxygenation to primarily the autoxidation product **6** in 27–44% yield.

(28) (a) Funabiki, T.; Mizoguchi, A.; Sugimoto, T.; Yoshida, S. *Chem. Lett.* **1983**, 917–920. (b) Funabiki, T.; Mizoguchi, A.; Sugimoto, T.; Tada, S.; Mitsuji, T.; Sakamoto, H.; Yoshida, S. *J. Am. Chem. Soc.* **1986**, *108*, 2921–2932.

(29) (a) Funabiki, T. In *Catalysis by Metal Complexes*; Funabiki, T., Ed.; Kluwer Academic Publishers: Dordrecht, The Netherlands, 1997; Vol. 19, pp 80–83. (b) As a caveat, it is not clear whether the above discussions are applicable to arene *cis*-dihydroxylation reaction catalyzed by Rieske "dioxygenases" (e.g., naphthalene dioxygenase, toluene dioxygenase). However, these so-called "dioxygenases" would appear not to be true dioxygenases in that they require NAD(P)H as a cofactor, presumably making them mechanistically more related to cytochrome P$_{450}$.

(30) Specifically, Sen concluded that, "While, from a practical standpoint, it is more desirable for both oxygen atoms of O$_2$ to be used for substrate oxidation, there appears to be no known catalytic system that operates as an artificial 'dioxygenase' under mild conditions toward 'difficult' substrates, such as those possessing unactivated primary C–H bonds." Lin, M.; Hogan, T.; Sen, A. *J. Am. Chem. Soc.* **1997**, *119*, 6048–6053.

Supporting Information Available: Stirring rate controls; the establishment of O$_2$ mass-transfer limitations; solvent vapor pressure correction example; two other representative O$_2$-uptake curves of kinetic runs of [VO(DBSQ)(DTBC)]$_2$ plus excess DTBC; presentation of the mechanism involving intact [VO-(DBSQ)(DTBC)]$_2$; figures showing how different mechanistic schemes give poor fits to the [VO(DBSQ)(DTBC)]$_2$ O$_2$-uptake data in Figure 1 in the main text; calculated catalyst reaction order using the chemical models in Scheme 2; the EPR of [VO-(DBSQ)(DTBC)]$_2$ and the EPR of [VO(DBSQ)(DTBC)]$_2$ with addition of a drop of DMSO; and Scheme S2, the electrophilic O$_2$ plus nucleophilic DTBC^{2-} semiquinone spectator alternative mechanism for step 2 in Scheme 3. This material is available free of charge via the Internet at http://pubs.acs.org.

JA052998+